International Conference on Space Optics—ICSO 2022

Dubrovnik, Croatia

3–7 October 2022

Edited by Kyriaki Minoglou, Nikos Karafolas, and Bruno Cugny,

Setup for high-precision wavefront measurements: design and technical limitations

Setup for high-precision wavefront measurements: design and technical limitations

Chris Britze*[a], Michael Vergöhl[a], Thomas Melzig[a], Stefan Bruns[a], Philipp Henning[a], Hans-Ulrich Kricheldorf[a], Luis Miguel Gaspar Venancio[b]

[a] Fraunhofer Institute for Surface Engineering and Thin Films, Bienroder Weg 54E, 30108 Braunschweig, Germany; [b]European Space Agency ESTEC, Noordwijk, The Netherlands

ABSTRACT

In broadband dielectric coatings, the wavefront of the reflected wave can change dramatically in a resonance-like manner as a function of wavelength. These wavefront errors can be a significant issue in high precision instruments. In the last years, effort has been undertaken to design and produce coatings to reduce these resonances. However, today there is still limited capability to characterize by measurement the spectral dependence of the wavefront error with high spectral resolution and accuracy. The goal of this paper is to present and analyze a design for a setup to measure the reflected wavefront from a coated flat component with high accuracy as a function of the wavelength. The proposed design is based on a passive system using high-precision off-axis parabolic mirrors. For sensing the wavefront error a Shack-Hartmann sensor is proposed, whose microlens array design is to be modified. According to error analysis and tolerance studies, the setup is capable of measuring wavefront distortion with sub-2 nm RMS accuracy within 510 nm to 950 nm. The angle of incidence and the polarization can also be varied without a loss of accuracy. In order to determine the point spread function (PSF) with high accuracy in addition to the wavefront measurement, the wavefront error of the setup itself needs to be below 50 nm RMS. The tolerancing performed in this study included the light source, shape errors of the mirrors, beam splitter, polarizers, and the sensors. Shape irregularities of the single elements were simulated by Zernike polynomials, and the residual wavefront error of the setup is estimated by Monte Carlo simulations, including uncertainties of the mechanical positioning. From these simulations, specifications for the mirrors have been worked out based on the goal of a system wavefront error lower than 50 nm RMS. The intended broad spectral range makes it challenging to identify a suitable Shack-Hartmann wavefront sensor. Different sensor configurations are evaluated experimentally, and a reproducible wavefront measurement can be achieved by adjusting the focal length of the microlens array. Thereby, the repeatability in wavefront measurements could be reduced from 3 nm to less than 1 nm RMS by modifying the microlens array parameters. Tilting the polarizer and beam splitter by 2° prevents ghost images and multiple reflections in the setup. Finally, considerations about the realization of a suitable reference measurement with an optical flat of sufficient surface quality are presented.

Keywords: Wavefront error, spectral, Hartmann-Shack sensor, beam splitter, optical coating

1. INTRODUCTION

The prevention of wavefront errors (WFE) is an essential goal for the optimal functionality of diffraction-limited optical systems. This goal is not new as, for example, Knowlden investigated this issue in 1981 [1]. WFE in optical systems are typically caused by a number of factors such as inhomogeneities of the used substrate and coating materials, surface errors of the components, bending stress etc. WFE may also occur due to thermal expansion in high-power laser applications [2] or result from stress induced by mounting the components. The wavefront error in dielectric beam splitter coatings can be surprisingly large, resonance-like errors of the reflected wavefront at certain wavelengths [3]. Also, interferometric measurements of multilayer coatings with non-uniform thickness may deviate at a wavelength other than the design wavelength [4]. Angus McLeod [5] also explained that convex shapes of optical components can look concave in some cases and vice versa. Modern beam splitters with a broad-band functionality and low loss can be produced by magnetron sputtering technology [6]. In a study funded by ESA it was found and explained that the group delay of the reflected light from a surface and its dispersion over the surface leads to the WFE resonances [7]. In that study a broader wavelength

range beam splitter coating with very low WFE was manufactured. The influence of resonances was reduced with a suitable choice of design. The wavefront error of the sample was determined by comparison with a reference substrate in a wavelength-dependent manner. Due to the longer measurement time, this sample was also measured with self-referencing. In this method, the wavefront error was determined for a specific wavelength used as a reference point, and only the wavelength was varied without removing the beam splitter. This method is faster, but limited by chromatic aberration effects in spectral range and accuracy [8].

2. MEASUREMENT SETUP

The data presented in the introduction lead to the conclusion that a relative measurement using a Shack-Hartmann sensor is a suitable approach. In a relative measurement, the sample is referenced to a component which has a known WFE. The requirements of the measuring system depend on the measuring object. The setup presented here is designed for measuring the "Euclid Dichroic" from the Euclid mission. The following table shows the essential requirements the setup should fulfil:

Table 1: Basic requirements for the measurement system.

Property	Value
Measurement type	Wavefront error and point spread function
Wavelength	510 - 950 nm or more
Spectral resolution	Better than 0.4 nm
Angle of incidence (AOI)	0° and 4°- 20°
Polarization	s and p
Sample shape and area	Flat, diameter $\leq$ 120 mm
Automation	Remote control
Illumination	No shadowing of sample area
Zernike polynomials	Z1 - Z55

The design can be based on a transmissive structure with lenses or a reflective structure with mirrors. The disadvantage of mirrors is that the aberrations are doubled when light is reflected from the surface. Lenses, on the other hand, can have chromatic errors, which is proven to be critical [7]. Thus, the focus in the present study is on the use of metallic mirrors.

Since shading effects are not desirable for the characterization of the optical components, measuring with a symmetrical Schwarzschild configuration is not a suitable solution. Off-axis mirrors were chosen as another option. The basic optical design of the WFE structure is shown in Figure 1.

The light from the source is monochromatized with a suitable system and coupled into the measuring system via a fiber. (element L in Figure 1). An aperture (A) reduces the diameter of the optical beam. The light is reflected from a parabolic off-axis mirror (M1), from which it is reflected in a parallel manner. The reduction of the beam diameter improves also the beam profile, which needs to be transformed from Gaussian to flat-top. The light is polarized with a crystal polarizer (P1). Another off-axis parabolic mirror (M2) expands the beam. Parallelization will be made by the next off-axis parabolic mirror (M3). The light is reflected from the sample S or from the reference substrate, which will be placed in the identical position. Mirrors M4 and M5 are identical to mirrors M3 and M2, respectively. P2 is the analyzer, which is identical to the polarizer P1. SH is the Shack-Hartmann sensor in the case of wavefront measurements between 4° and 20°. The sensor part of the bench is mounted together on a rotating arm. For measurements at different angles, the sensor part can be rotated around the axis of the sample (Figure 1) without changing the relative configuration of these elements.
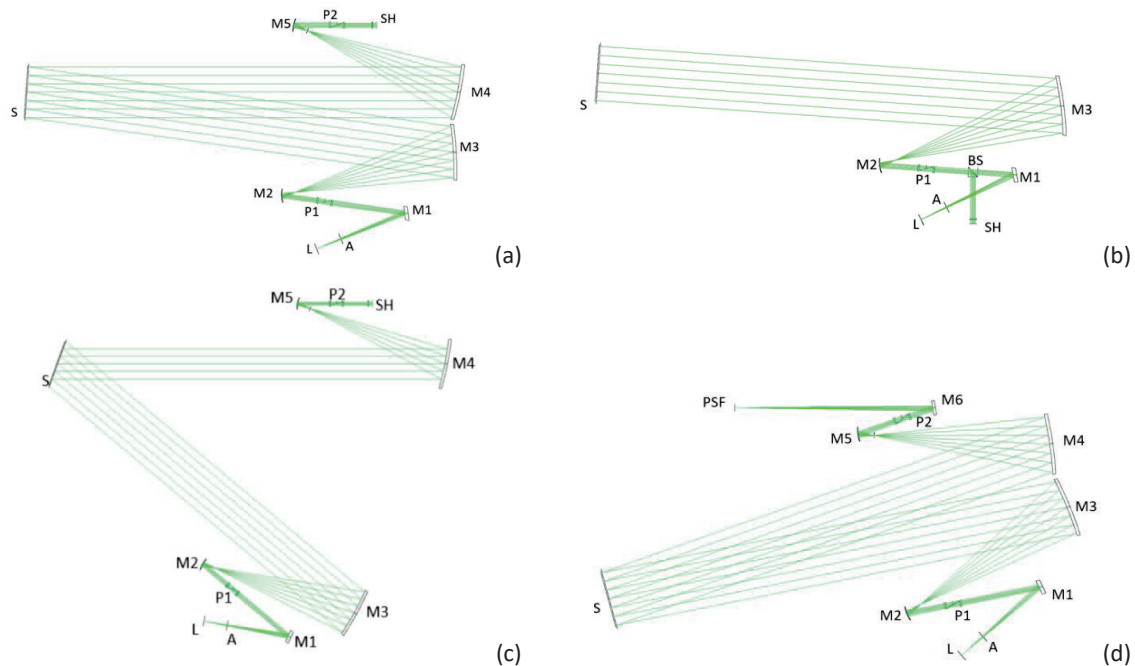
Figure 1: Optical setup of the bench for the wavefront measurement at 4° AOI (a), 0° AOI (b), at 20° AOI (c) and for the PSF measurement at 20° AOI (d).

The WFE measurements at normal incidence will be performed in retro-reflectance mode. For these measurements, the system is expanded with another beam splitter. This causes the light reflected from the sample to couple out into the Shack-Hartmann sensor. In the case of PSF measurements (d) the Shack-Hartmann sensor will be removed, and a focusing off-axis mirror (M6) and the PSF camera will be inserted manually. Again, for the 0° measurement no polarizer and analyzer is needed, but a beam-splitter. The components of the measurement system are described in more detail below.

2.1 Light source L

A light source with very good imaging properties is required for the wavefront measurement. As light source, a broadband laser is proposed. There are two main disadvantages of a laser. One is a relatively high price, and the other is the higher noise and lower stability of the laser compared with, for example, a tungsten lamp. The visible stability is ± 0.5% in the range of milliseconds to seconds according to the manufacturer [9]. On the other hand, there are big advantages of a laser source. The most important ones are the high intensity and the good beam quality. With the high spectral power of the laser, the spectral bandwidth of the measuring beam can be reduced if the intensity is sufficient. A flat top beam can be realized by using only the middle part of the beam (i.e. cutting off the outer area). Otherwise, a beam shaping module would be needed, which would complicate the optical setup. The beam quality is also an important point. Neither a tungsten-halogen, nor a laser-arc source can be expected to deliver nearly monomode beam quality, which would lead to degradation of the image properties. A suitable option for the white light laser would be a "SuperK FIANIUM" by NKT photonics. This light source emits a light spot with a low divergence angle of < 1 mrad in the wavelength range from 410-2400 nm. This type of laser is available with different power levels, delivering up to 5 mW/nm in a FIU-15. The light from the laser can be monochromatized based on holographic transmission gratings in a Laser Line Tunable Filter (LLTF). The monochromator is connected to the measurement system with a monomode fiber, from which the light emerges with a numerical aperture of NA = 0.09 to 0.17, depending on the wavelength. The estimated power from the fiber of a white light laser with a modified LLTF and the intensity distribution on the sample is shown in Figure 2.
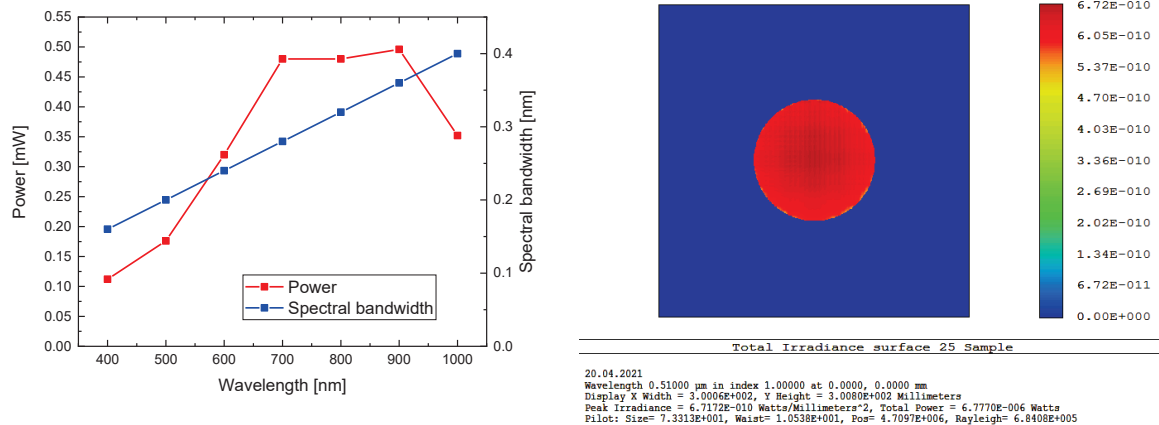
Figure 2: Estimated spectral bandwidth (blue) and performance of the FIU-15 and modified LLTF (left). 2D distribution of the incident light on the substrate (right). The strongest deviation on the sample in X direction: 5% and Y direction: 7%.

2.2 Beam splitter BS

For a measurement at 0°, the reflected beam must be separated from the incident beam. This separation can be done with the help of a beam splitter cube. In the selected wavelength range, it should transmit the measuring beam with 50% and deflect it by 90° with 50%. In addition, the ratio should also be the same for p- and s-polarization. If the cube deviates from this ideal ratio, the efficiency of the beam splitter decreases, because less light is coupled into the sensor. To avoid multiple reflections between the cube and the other components, the cube is tilted by 2°. The acceptance angle of the beam splitter should be designed for this setting. The adjustment can be controlled with the help of a turntable. To avoid multiple reflections in the cube itself, the four optical sides must be anti-reflective ($R_{avg} < 0.6\%$, $R_{abs} > 1\%$). The beam splitter cube is available with a clear aperture of 20 mm. The wavefront error of the cube has to be limited since it contributes to the overall error of the setup. A beam splitter with interferometer quality is preferable here.

2.3 Polarizer P

Since the wavefront error is also polarization dependent, the polarization angle of the beam should be set for an accurate measurement. A Glan-Thompson polarizer is suitable for this. Dichroic polarizers, with wavelength-dependent resonances, could introduce large wavefront errors into the system. They are unsuitable. Glan-Taylor polarizers create an internal ghost due to an air gap and are therefore also unsuitable. Glan-Thompson polarizers are available in interferometer quality (wavefront distortion of $\lambda/10$) and a clear aperture of 12.6 mm. Since the free aperture of the component limits the maximum size of the beam, all other imaging components such as mirrors or lenses must be matched. In order to avoid multiple reflections to other components here as well, the polarizer is tilted by -2° using a rotating platform. The acceptance angle of the polarizer should also be designed for this setting. The position of the polarizer can be adjusted via a motorized turntable. During a calibration procedure, the optimal setting for p- and s-polarization must be found before the wavefront measurement. An intensity measurement at the Brewster angle of a quartz glass is suitable for this.

2.4 Sample holder S

For exact mounting, the substrate should be positioned on polyetheretherketone (PEEK) rollers and adjusted using positioning platforms. To protect the substrate, the holder is equipped with PEEK edge protectors. This ensures that the substrate does not come into contact with metal. The substrate can be stored standing on rollers. The expected surface deformation of the substrate due to gravity was estimated to be at maximum 0.25 nm with help of a COMSOL simulation. In addition to the roll diameter and substrate thickness, the material properties are important parameters for the simulation. The sample holder (left) and the deformation in the Z direction (right) are shown in Figure 3 below.
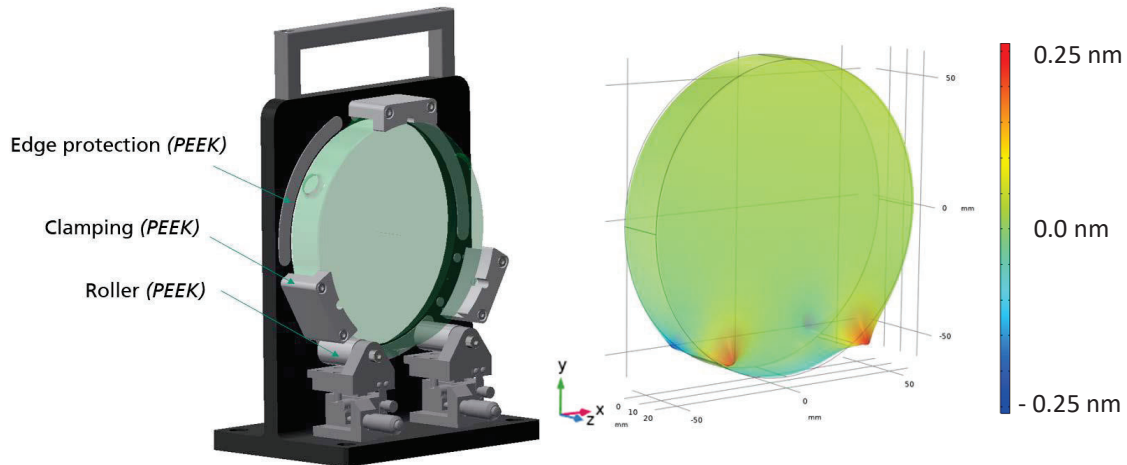
Figure 3: Specimen holder with positioning platform (left), simulated surface deformation in the Z direction (right).

3. LIMITATIONS OF THE MEASUREMENT SYSTEM

3.1 Referencing

Since wavefront measurements are relative measurements, the setup must be calibrated using a reference substrate. The reference substrate is a flat surface that is precisely measured. It is not coated with a dielectric filter, so the wavefront error in reflection is only dependent on the surface of the substrate and not on the wavelength. In the calibration, the reference substrate is measured instead of the sample substrate. If this calibration is done manually, system changes such as vibrations or air turbulence can be generated, which is why a motorized setting is preferable here. This makes it easy and quick to change between the sample and the reference. The default settings for optimal positioning can also be saved by the system. The sample turntable with reference and sample is shown below in Figure 4.
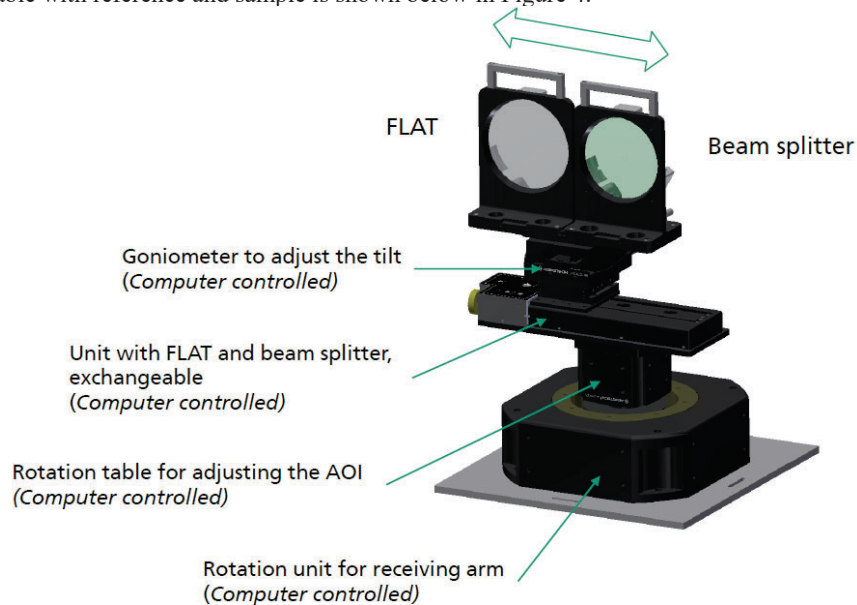

Figure 4: Turntable with reference and sample for automated switching between both substrates.

The measurement accuracy of the substrate wavefront error is limited by the calibration accuracy of the measurement system. In order to increase the accuracy, the measurement of the reference substrate is of particularly high importance. The flatness of the sample could be determined with an interferometric calibration measurement. The measurement is based on a Fizeau interferometer that can measure surfaces with a diameter of up to 300 mm. The extended measurement accuracy (k = 2 corresponds to ±2 sigma) is 11 nm peak to valley (PtV) [10]. This means that 95.45% of the measurement data points are within 11 nm. The standard deviation of the calibrated surface deviation is therefore σ = 2.75 nm PtV. The contribution to the wavefront error would be 5.5 nm (1σ) (PtV), since the reflection doubles the contribution. This corresponds to 1.1 nm RMS, assuming that RMS error = PtV/5. In order to avoid errors when holding the sample, the flat is measured in the holder used during calibration.

3.2 Shack-Hartmann sensor

A Shack-Hartmann sensor is recommended to determine the deformation of the wavefront. Within this sensor, a microlens array is positioned in front of an image sensor such as a CCD or CMOS array. If the incoming wave hits the microlens array at an angle due to the wavefront error, the spots behind the individual lenses are deflected. The spatial deviation of the spots between the measurement of the reference substrate and the sample can then be used to reconstruct the wavefront. With an evaluation software, the wavefront error can be approximated with Zernike polynomials. In order to increase the sensor accuracy in the measuring range, the focus length of the microlenses, number of microlenses and lens pitch should be optimized. The required minimum number of lenses (N) depends on the mode (M) of the Zernike polynomials and can be determined with the equation $2N \geq M$ [11]. Since high frequency errors of the sample should also be measured, an approximation with up to 55 Zernike polynomials is important. This degree of polynomials corresponds to M = 9, so at least 18 lenses should be illuminated. Using more microlenses can reduce the scanning error and thus the reconstruction error until the numerical errors are in the same order of magnitude as the scanning error [11]. Therefore, a higher number of microlenses is preferable. When projected onto the sensor, the image of the substrate is downscaled by a factor of 11. In a sensor with a lens pitch of 150 μm, 71 lenses are illuminated in one direction at an angle of incidence of 0°. The focal length of the microlens array determines how sensitive the sensor reacts to the wavefront error. Arrays with smaller focal lengths can measure higher slopes in the wavefront errors. The longer the focal length, the finer the effect of wavefront errors and the more stable the measurement results can be determined [12]. However, the focal length cannot be designed too long, otherwise wavelength-dependent diffraction effects from the microlens array may occur. For example, an orthogonal array with a lens pitch of $d = 150$ μm and a focal length of $f = 13$ mm can generate stable measurements in the UV range, but cannot measure accurately in the NIR range due to disruptive diffraction effects. The spot image on a Shack-Hartmann sensor for the wavelength $\lambda = 1064$ nm is shown in Figure 5 below. In addition to the diffraction images in the spots, the image with a focal length of 13 mm is also overlaid with other diffraction images.
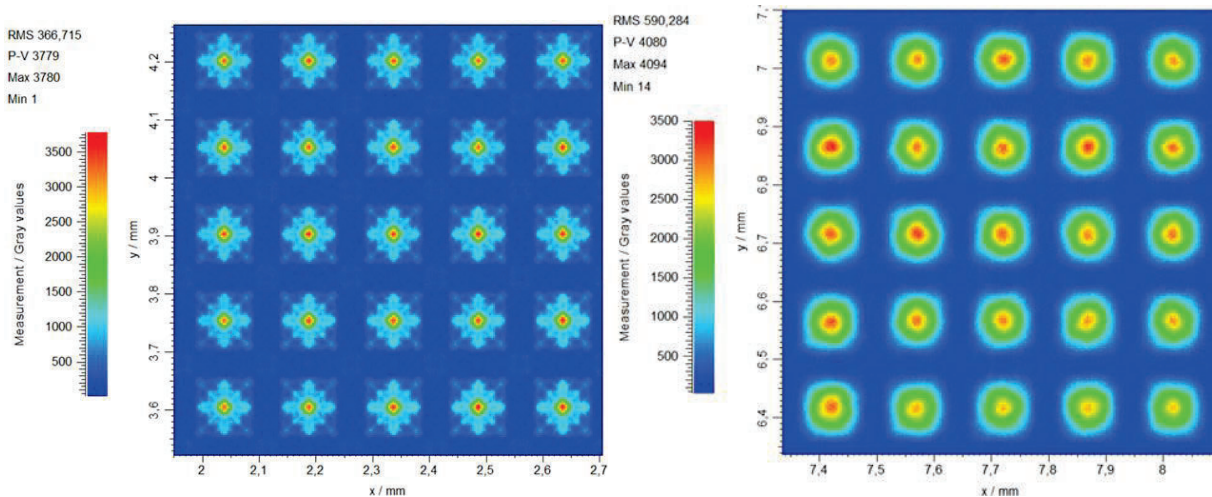

Figure 5: Spot image measured on Optocraft's Shack-Hartmann sensor UHR3 at a wavelength of 1064 nm. The array's lens pitch is 0.15 mm and the focal length is $f = 13$ mm (left) and $f = 9.5$ mm (right).

Based on these results, the reproducibility was subsequently determined for a self-assembled Shack-Hartmann sensor together with Optocraft. The lens array was selected with a focal length of f = 9.5 mm and a pixel pitch of 150 µm. Not only the lens array is important for the reproducibility and accuracy of the wavefront sensor, but also the image sensor properties such as pixel size, signal noise ratio (SNR) and bit depth are important parameters. The CMOS sensor IMX367 from Sony with a pixel size of 3.45 µm × 3.45 µm, 12 bit depth and an SNR of 1:4478 was used as the image sensor. The repeatability, the difference between two measurements, was determined three times at three different wavelengths. 66 lenses were used for the measurement. The maximum deviation in this measurement was 0.97 nm RMS. The data determined are shown in the Table 2 below. According to the Optocraft, this image sensor with a microlens pitch of 0.13 and a focal length of 3.3 mm has a repeatability of 3 nm in the same wavelength range [13].

Table 2: Determined repeatability of the sensor configuration: focal length 9.5 mm; lens pitch 0.15 mm; pixel size 3.45 µm x 3.45 µm for the Wavelength 532 nm, 635 nm and 1064 nm.

Wavelength [nm]	Repeatability 1 [nm]	Repeatability 2 [nm]	Repeatability 3 [nm]	Mean Repeatability [nm]
532	0.74	0.72	0.70	0.72
635	0.90	0.87	0.97	0.91
1064	0.80	0.73	0.81	0.78

3.3 Ghost images

Ghost images can lead to possible errors in the wavefront measurement. The main reasons of ghost images, like the polarizer and the beam splitter, can be eliminated by tilting the components. Nevertheless, there are other contributions that cannot be prevented so easily. Therefore, a ghost image analysis was performed for the measurement system by using the TracePro software. Radiation components with a minimum of 10^{-7} of the input intensity were tracked in the simulation. Beams with a lower intensity are not tracked and are no longer included in the simulation. At an AOI of 0°, the Shack-Hartmann sensor has a ghost image with 1.43% of the intensity of the main image. The main part is caused by multiple reflections at the beam splitter. This result can only be achieved by anti-reflective coatings on all optical surfaces of the beam splitter (R_{avg} < 0.6% and R_{abs} < 1%). A ghost of 0.03% was determined for the measurements with an AOI of 4° - 20°. This low ghost value can only be achieved because no beam splitter is needed at a higher angle of incidence.

3.4 Measurement accuracy

To determine the influence of the ghost and the accuracy of the sensor, the Shack-Hartmann spot image of a deformed wavefront was simulated with the software ZEMAX. Before evaluating the spot image with the Shack-Hartmann evaluations software SHS Works from Optocraft, it can be optionally superimposed with an artificial ghost image of 1.43% intensity. The determined wavefronts were compared with each other and with the wavefront entering the ZEMAX simulation. The array had a focal length of 9.5 mm and a lens pitch of 150µm. The measurement system was described with the Zernike polynomials 1-36 and a wavefront error of 531 nm PtV and 98.5 nm RMS in ZEMAX. The sample was described with the Zernike polynomials 1-55 and a wavefront error of 317.85 nm PtV and 76.62 nm RMS. A ghost image was superimposed on both the reference image and the sample image. The determined wavefront error is strongly dependent on the parameters in the evaluation software (threshold, pixel for a peak, offset etc.). In a direct comparison, the determined wavefront error with a ghost image is 0.11 nm PtV higher than the evaluation without a ghost image. The RMS wavefront error between the spot image with ghost and without ghost is the same within the framework of the simulation accuracy. The wavefront error used for the simulation is 0.94 nm RMS higher than the wavefront error evaluated with a ghost image. Figure 6 compares the wavefront error before simulating the sensor (left) and after simulating the sensor and reconstructing it using the SHS Works software.

WFE entered Zemax
317,85 nm PtV ; 76,62 nm RMS

WFE determined in SHS Works
320,21 nm PtV; 75,68 nm RMS

Simualtion of spot image
with ZEMAX

Evaluation of spot image
with SHS Work

```
7.72E-006
6.95E-006
6.17E-006
5.40E-006
4.63E-006
3.86E-006
3.09E-006
2.32E-006
1.54E-006
7.72E-007
0.00E+000
```

```
Total Irradiance surface 51 Sensor
09.08.2022
Wavelength 0.95000 μm in index 1.00000 at 0.0000, 0.0000 mm
Display X Width = 1.4298E+001, Y Height = 1.4300E+001 Millimeters
Peak Irradiance = 7.7167E-006 Watts/Millimeters^2, Total Power = 5.8144E-005 Watts
Pilot: Size= 3.8085E+001, Waist= 3.8085E+001, Pos= 0.0000E+000, Rayleigh= 4.7967E+006
```
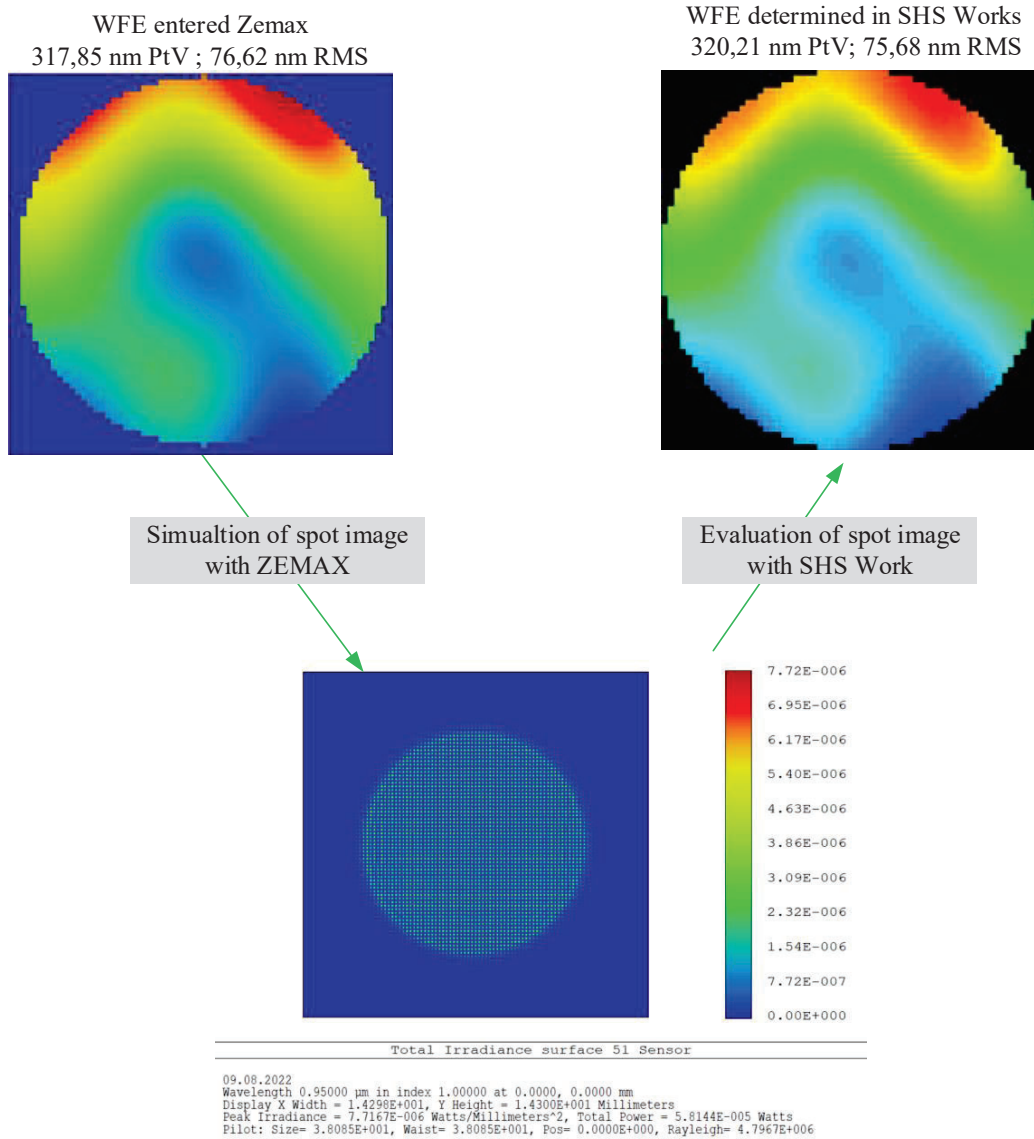
Figure 6: Workflow to determine the accuracy of the sensor and the influence of a ghost image. A spot image is simulated in ZEMAX with an incoming wavefront error. The SHS Works software is used to reconstruct the wavefront, including the ghost, from the simulated spot image.

The minimum achievable measurement uncertainty can be estimated by considering the results listed above. The measurement reliability of the calibration with the reference substrate (σ_{cal} = 1.1 nm RMS), the reproducibility of the sensor (σ_{rep} = 0.91 nm RMS) and the measurement accuracy of the ghost analysis (σ_{acc} = 0.94 nm RMS) must be considered. According to equation (1) these values can be combined to a minimum measurement uncertainty of 1.74 nm RMS.

$$WFE_{\text{uncertainty}} = \sqrt{\sigma_{cal}^{\ 2} + \sigma_{rep}^{\ 2} + \sigma_{acc}^{\ 2}} \tag{1}$$

$$WFE_{\text{uncertainty}} = \sqrt{(1.1\text{ nm})^2 + (0.91\text{ nm})^2 + (0.94\text{ nm})^2} = 1.71\text{ nm}$$

3.5 System wavefront error

For more information about the wavefront distortion, the point spread function of the substrate should be measured. In order to keep the influence of the device on the wavefront measurement and point spread function measurements as low as possible, a small wavefront error in the measurement system is preferable. The expected wavefront error was estimated using a Monte Carlo simulation in ZEMAX. The optical components (lenses, mirrors, beam splitters and polarizers) are subject to positioning inaccuracies and shape deviations. The surface shape deviations of the mirrors were generated in ZEMAX with the operand TEZI (Z5-Z36). The Zernike coefficients are chosen from a uniform distribution and then scaled to produce the desired surface form error of 12 nm RMSi. Surface defects (e.g. scratches, dents, etc.) cannot be simulated. Mirrors with such small surface deviations can be made with an electropolished NiP layer. A mirror with a shape deviation of 20 nm RMSi and a diameter of 320 mm was already manufactured in 2014 [14]. Due to the smaller diameter and the iterative manufacturing process, such surface variations are feasible for companies like Spaceoptix. The polarizer and beam splitter can be made with a wavefront error of $\lambda/10$. Since the surfaces are flat, only a long-period error (astigmatism and spherical aberration) without power error was assumed. As position uncertainty it was assumed that the light source and the small mirrors can be adjusted in the XY direction with ±3.5 µm and in the Z-direction with ±4.4 µm. This uncertainty corresponds to the path with a 10° turn of the adjustment screw with a pitch of 254.0 µm/rev for the X-Y-direction and 318 µm/rev for the Z-direction. Due to their weight, the size of mirrors or lenses in the structure can only be adjusted using stages with micrometer screws. Therefore, the uncertainty in the X-Y-Z-direction was estimated to ±5 µm.

For the estimation of the system's total wavefront error, 200 different cases of settings and surface deviations were examined. The maximum of the distribution at 4°-20° wavefront measurement is at 43.5 nm RMS. There is no significant difference in the RMS wavefront error of the system when the sample is measured at an angle of incidence of 4 or 20°. The wavefront error of the system at 0° is slightly higher with 66.5nm RMS. The reason for this is that the same optics are used in the returning beam as in the incoming beam and errors in the adjustment or in the optics have a greater impact. The maximum of the distribution of the system wavefront error for the point spread function measurement is 45.3 nm. This value is higher compared to the other measurement configurations due to an additional mirror.
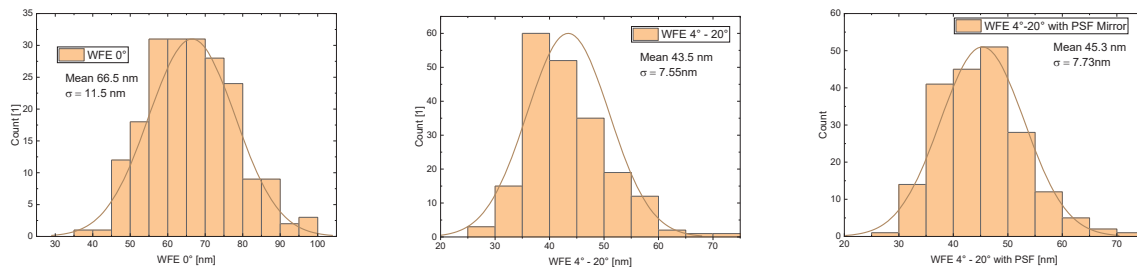

Figure 7: Distribution of the wavefront error in the system for the angle of incidence 0° AOI (left), for wavefront measurements with 4-20° AOI (middle) and for measurement from the point spread function with 4-20° (right).

4. CONCLUSION

In this work, a step-up for a measurement system was presented that allows the spectral measurement of the wavefront error of a dichroic filter. The challenges of the components like light sources, beam splitters, polarizers, substrate holder, referencing and sensors were described in detail. The limits of the measurements have been investigated. The choices for the design of the Shack-Hartmann sensor were explained in more depth. The reproducibility of a Shack-Hartmann sensor was determined. The measurement accuracy of the wavefront was determined using a simulated spot image of a known wavefront. In addition to these sources of error, the calibration is also decisive for the uncertainty of the measuring system. The limits of the measurement uncertainty of the setup were estimated at 1.74 nm. The total wavefront error of the system was estimated by Monte Carlo simulations different measurement setups. The maximum of the distribution was 66.5 nm for measurements at normal incidence and 43.5 nm for measurements at 4°- 20° AOI. The condition for this small error is an optimally adjusted optical system. These results can be helpful for the design of future wavefront measurement systems.

REFERENCES

[1] Knowlden, R. E., "Wavefront errors produced by multilayer thinfilm optical coatings", AA (Arizona Univ., Tucson), Ph.D. Thesis Arizona Univ., Tucson. (1981).

[2] Cho B., Danielewicz E. J. & Rudisill J. E., "Absorption measurement of high-reflectance coated mirrors at 193 nm with a Shack–Hartmann wavefront sensor", Optical Engineering 51(12), 121803 (2012).

[3] Venancio, L. M. G., Carminati, L., Alvarez, J. L., Amiaux, J., Bonino, L., Salvignol, J. C., Vaverk R. Laureijs R., Short A., Boenke T., & Strada, P., "Coating induced phase shift and impact on Euclid imaging performance", Space Telescopes and Instrumentation 2016: Optical, Infrared, and Millimeter Wave. Vol. 9904. SPIE, (2016).

[4] Baumeister P. W., "Optical Coating Technology", SPIE Press (2004).

[5] McLeod A., "Phase Matters - Proper coating design and fabrication requires a good understanding of phase", Optical Design & Engineering, oemagazine, SPIE Newsroom (2005).

[6] Lappschies, M., Weber, T., Venancio, L., & Jakobs, S, "Advanced dielectric coatings for the Euclid mission telescope manufactured by the PARMS process," Optical Interference Coatings. Optical Society of America, (2016).

[7] Vergöhl, M., Britze, C., Bruns, S., Ahrens, J., Schäfer, B., Mann, K., & Kirschner, V., "Development of a broadband dielectric beam splitter with reduced spectral wavefront error", Advances in Optical Thin Films VI. Vol. 10691. SPIE, (2018).

[8] Mann, K., Schäfer, B., Zimara, J., Vergöhl, M., Britze, C., Bruns, S., & Kirschner, V., "Spectrally resolved wavefront measurements on broad-band dielectric coatings.", Laser-Induced Damage in Optical Materials 2018: 50th Anniversary Conference. Vol. 10805. SPIE, (2018).

[9] NKT Photonics, "SUPERK FIANIUM – Pulsed white light laser platform – technical specification", (2022).

[10] Ehret G., Reinsch H., Schulz M., "Interferometric and deflectometric flatness metrology with nanometre measurement uncertainties for optics up to 1 metre at PTB.", Optical Metrology and Inspection for Industrial Applications VI. Vol. 11189. SPIE, (2019).

[11] De Oliveira, O. G., & de Lima Monteiro, D. W. "Optimization of the Hartmann–Shack microlens array", Optics and Lasers in Engineering, 49(4), 521-525, (2011).

[12] Neal, D. R., Copland, J., & Neal, D. A. "Shack-Hartmann wavefront sensor precision and accuracy.", Advanced Characterization Techniques for Optical, Semiconductor, and Data Storage Components. Vol. 4779. SPIE, (2002).

[13] Optocraft, "SHSCam UHR3-130-GE – technical specification", (2021).

[14] Gebhardt, A., Beier, M., Scheiding, S., Peschel, T., & Löscher, H. "Fabrication method for large off-axis aspherical metal mirrors", 14th International Conference & Exhibition of the European Society of Precision Engineering and Nanotechnology, Dubrovnik, Croatia (pp. 2-6) (2014).